

# Experimental and Numerical Studies of Flows About a Toroidal Ballute

I. Lourel<sup>1</sup>, T.N. Eichmann<sup>1</sup>, S. Isbister<sup>2</sup>, T.J. McIntyre<sup>1</sup>, A.F.P. Houwing<sup>2</sup>, and  
R.G. Morgan<sup>1</sup>

<sup>1</sup> Centre for Hypersonics, The University of Queensland, Brisbane, 4072, Australia

<sup>2</sup> Aerophysics and Laser-based Diagnostics Research Laboratory, Department of  
Physics, Australian National University, ACT, 0200, Australia

**Abstract.** Experiments have been conducted to investigate flows around a toroidal ballute and a towed ballute-spacecraft system. Fluorescence imaging and thermometry measurements were used to visualize and obtain temperature maps of the flow fields. The separation length between the ballute and the spacecraft was varied and both steady and unsteady flow fields were observed. Heat transfer measurements, PLIF images and CFD results are presented.

## 1 Introduction

A recent review by Hall [1] on the use of ballutes for planetary flights has suggested that 10–100 m diameter ballutes towed behind a spacecraft can form the basis of a feasible planetary aerocapture mission concept. Feasibility studies are being carried out for missions to Mars, Venus, Saturn, Titan, Neptune and Pluto. Although ballute prototypes have been flight tested on Earth and on Mars, fundamental uncertainties and technical issues remained unresolved and extended flight and wind tunnel testing is required [1].

A ballute (*balloon parachute*) is used as a lightweight, deployable drag device. Many different ballute designs have been proposed since its invention in the 1960s. Successful tunnel testing [2] of a towed toroidal ballute-spacecraft system has recently been performed in the GALCIT T5 Hypervelocity Free Piston Shock Tunnel [3] utilizing mission conditions of the Mars Microsatellite and the Titan Organics Explorer (see Table 1 for mission parameters). Heat flux measurements at various locations on the ballute and at the stagnation point of the spacecraft were recorded and flow visualizations were done via shadowgraph.

This work showed that steady flow could be achieved where the shock and wake produced by the leading spacecraft passed through the opening of the toroidal ballute and interacted with the ballute bow shock well downstream. Attempts were made to produce unsteady flow. The first attempt involved moving the spacecraft forward with respect to the ballute and the second attempt involved blocking the opening of the toroid. Irregularities in the spacecraft bow shock were observed for the first case, which indicated the possibility of small-amplitude unsteadiness. For the second case, a peculiar shock pattern was evident, with a clear indication of unsteady flow.

The present study focuses on the effect of a large variation of the ballute-spacecraft separation length on heat transfer and flow stability. Heat transfer and pitot pressure measurements were taken for three different ballute-spacecraft separation lengths. Flow fields were visualized using Planar Laser Induced Fluorescence (PLIF) imaging. The temperature field and shock locations deduced from the images were compared with perfect gas CFD simulations.

**Table 1.** Possible ballute mission design parameters

	Mars Micro- satellite	Venus Sample Return	Titan Organics Explorer	Neptune Orbiter
Flight Density ( $\text{kg.m}^{-3}$ )	$7.1 \times 10^{-7}$	$2.2 \times 10^{-7}$	$1.9 \times 10^{-7}$	$6.0 \times 10^{-9}$
Flight Velocity ( $\text{m.s}^{-1}$ )	5490	10600	8550	26900
Overall Ballute Dia. (m)	18	180	65	180

## 2 Experimental Work

### 2.1 T3 Free-Piston Shock Tunnel Facility

All experiments were performed in the T3 Free-Piston Shock Tunnel Facility at the Australian National University. Two operating conditions were used in the experiments. The moderate enthalpy condition (4.0 MJ/kg) was used for most of the experiments while the lower enthalpy condition (2.4 MJ/kg) was used to allow comparison with perfect gas CFD simulations of the flow. The free-stream conditions calculated at the nozzle exit are given in Table 2. A 305 mm exit-diameter conical nozzle with 25.4 mm throat and  $7.5^\circ$  internal half angle was used. The nitrogen test gas was mixed with 0.5%  $\text{O}_2$  to obtain sufficient nitric oxide (NO) for fluorescence imaging. The underlying theory and a detailed description of the experimental setup of the PLIF system can be found in [4].

**Table 2.** Freestream conditions in the T3 Shock Tunnel

	Moderate Enthalpy 4.0 MJ/kg	Low Enthalpy 2.4 MJ/kg
Density ( $\text{kg.m}^{-3}$ )	0.030	0.051
Velocity ( $\text{m.s}^{-1}$ )	2700	2100
Pressure (kPa)	3.1	3.0
Temperature (K)	347	200
Mach Number	7.5	7.1

## 2.2 Model and Instrumentation

Figure 1 shows the ballute-spacecraft model used, which was scaled from the model used by Rasheed et al. [2] in their experiments. A metal ring (112 mm in diameter) was used to represent a rigid toroidal ballute and a sphere (12.7 mm diameter) mounted on a cylindrical sting was used to represent the leading spacecraft. The separation length  $d$  is adjusted by sliding the spacecraft sting in and out of the main conical support. The model was instrumented with a fast response coaxial thermocouple and a PCB pressure transducer at the locations shown. The thermocouple was based on a design by Sanderson [5]. Nominal thermal properties were used to deduce heat transfer rates instead of direct calibration.

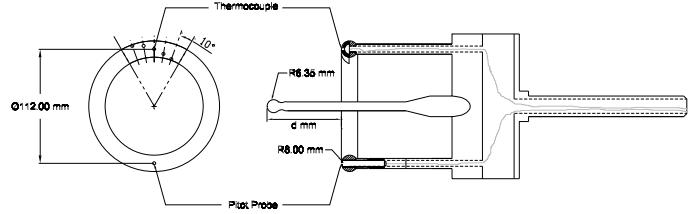


**Fig. 1.** The ballute-spacecraft model

Experiments were performed using the ballute model with and without the leading spacecraft. Ballute-spacecraft separation lengths used were  $d = 56, 81$  and  $148$  mm for the moderate enthalpy condition and  $110$  mm for the low enthalpy condition.

## 3 Results and Discussion

### 3.1 Flow Patterns Around a Toroidal Ballute

Figure 3 shows a PLIF image of flow around the toroidal ballute model at the moderate enthalpy condition. It can be seen that the conical shock has converged to form a Mach disk downstream of the opening. A similar flow pattern was observed by Riabov [6] in his study of toroids. A torus having a sufficiently large  $H/R$  value (see Fig. 2(b)) was found to produce a similar shock pattern to that shown in Fig. 3, while one with  $H/R = 1$  produced flow features of a stream near a bluff disk. In the first case (large  $H/R$  values), the stagnation points would be close to the front points of the torus while in the second case (small  $H/R$  values), the location of the stagnation points would be difficult to predict [6].

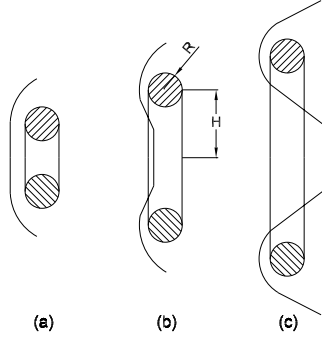


**Fig. 2.** Flow patterns around toroids having different  $H/R$  values

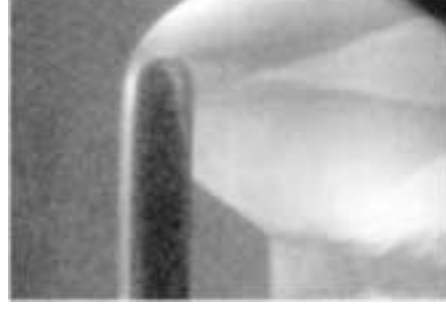


**Fig. 3.** PLIF image showing flow around the ballute

### 3.2 Steady Flows Around a Ballute and Spacecraft

Steady flows were observed for ballute-spacecraft separation lengths of 56 and 81 mm (see Figs. 4 and 5) at the moderate enthalpy condition. For both configurations, the interaction took place downstream of the frontal surface of the ballute and no irregularities in the flow fields were observed. Both heat transfer and pitot pressure measurements confirmed the establishment of steady flows.

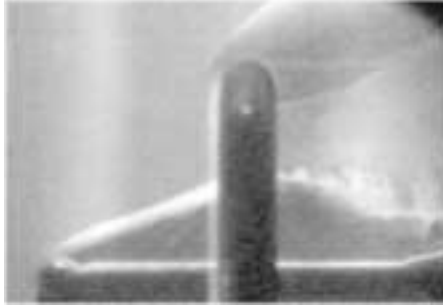


**Fig. 4.** PLIF image showing flow around the ballute and spacecraft ( $d = 56$  mm)

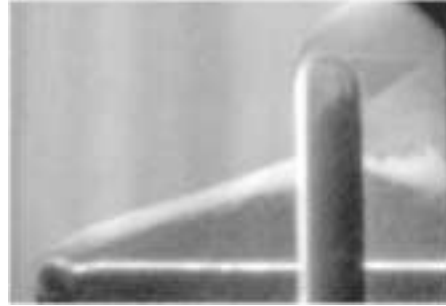


**Fig. 5.** PLIF image showing flow around the ballute and spacecraft ( $d = 81$  mm)

### 3.3 Unsteady Flows Around a Ballute and Spacecraft

For a separation length of 148 mm, the shock-shock interaction occurred near the stagnation streamline of the toroidal bow shock. From the PLIF images, it was concluded that the boundary layer on the spacecraft sting separated and traveled upstream. At the joint to the spherical spacecraft, the separation shock (see Fig. 6) was thought to have merged with the expansion waves and the recompression shock which both originated at the joint. This interaction was

thought to have strengthened the spacecraft bow shock and caused the shock to expand outwards radially (see Fig. 7). Here, it should be noted that the conical support of the spacecraft sting was situated slightly further downstream compared to Fig. 6 and hence the orifice blockage was somewhat reduced.

The distinct unsteadiness of the flow can also be witnessed in the heat transfer (§3.4) and pitot pressure measurements. Further explanation regarding the dynamics of the flow field can be found in [4].

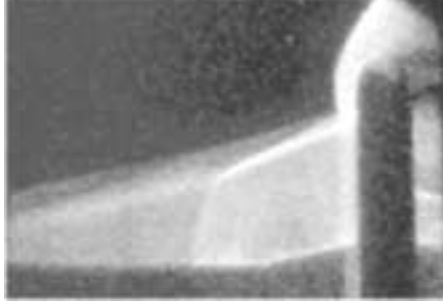


**Fig. 6.** PLIF image showing the separation shock ( $d = 148$  mm)

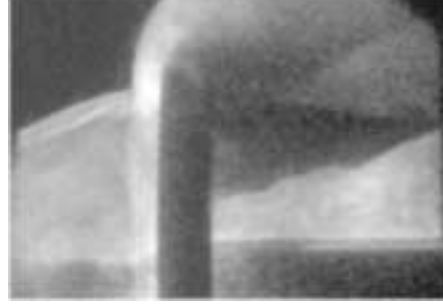


**Fig. 7.** PLIF image showing the expanded spacecraft bow shock ( $d = 148$  mm)

The unsteady flow field showed resemblance to the choked flow obtained in an experiment by Rasheed et al [2]. In their experiment, a plate was used to block the opening of the ballute in an attempt to produce unsteady flow. Peculiar shock patterns were observed where the spacecraft bow shock ballooned out and the combined shock swallowed the ballute.

### 3.4 Comparison between Steady and Unsteady Flows

The theoretical heat flux on the ballute was calculated using the Fay–Riddell theory for stagnation point heat transfer on a cylinder [7]. The expression reduces to [2]

$$\dot{q} = 0.570Pr^{-0.6}\sqrt{\rho_o\mu_o K}(C^*)^{0.1}h_o \quad (1)$$

where  $Pr$ ,  $\rho$ ,  $\mu$ , and  $h$  represent the Prandtl number, density, viscosity and specific enthalpy respectively. Also

$$C^* \approx 0.5^{-1/3} \text{ and } K \approx (V_\infty/D)\sqrt{8\rho_\infty/\rho_e}$$

where  $V_\infty$  represents the freestream velocity and  $D = 16$  mm is the cross-sectional diameter. Subscripts ‘ $o$ ’, ‘ $\infty$ ’ and ‘ $e$ ’ represent the stagnation, freestream and boundary layer edge conditions respectively. For the moderate enthalpy condition, the calculated stagnation point heat flux is  $4.8 \text{ MW/m}^2$ , which is in close agreement to the measured values for the steady flow case (see Fig. 9).

Figures 8 and 9 show selected temperature data and the corresponding computed heat flux for model configurations  $d = 81$  mm (steady flow) and 148 mm (unsteady flow). From the oscillations observed, it is clear that the interaction between the spacecraft and the ballute shocks caused the flow to become unsteady.

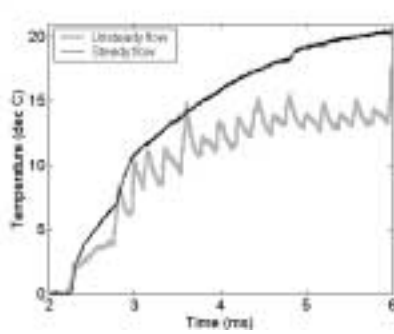


**Fig. 8.** Temperature history

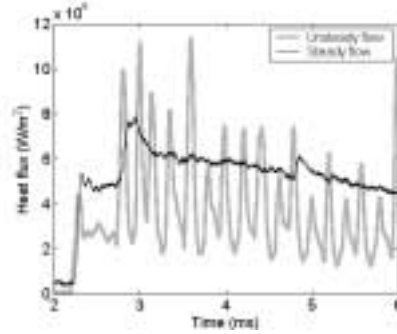


**Fig. 9.** The corresponding surface heat flux history

### 3.5 Comparison with CFD

Temperature fields around the ballute and spacecraft were obtained at the low enthalpy condition. PLIF images were recorded using  $J = 6.5$ , 18.5, and 28.5 levels (where  $J$  represents the different rotational levels in the ground state) and were combined to give the composite temperature map shown in Fig. 10(a). The CFD-FASTRAN simulation produced shock locations and temperature fields which are in good agreement with the experimental result (see Fig. 10(b)) for most of the flow. Here the ballute is truncated along the vertical plane of symmetry for ease of visualization.

## 4 Conclusions

As pointed out by Hall [1], considerable work remains to be done to verify the feasibility of the ballute concept. In brief, the present work addressed issues regarding ballute shape ( $H/R$  ratio), heating and stability.

Experiments have been carried out to reveal the intricate flow patterns around the toroidal ballute and the ballute-spacecraft system. The results presented here confirmed the feasibility of a steady flow for a towed toroidal ballute and gave a preview into the complex flow phenomenon in the case of an unsteady flow. Fluorescence imaging and thermometry measurements have been utilized not only to give a visualization of the flow field but to give useful quantitative data.

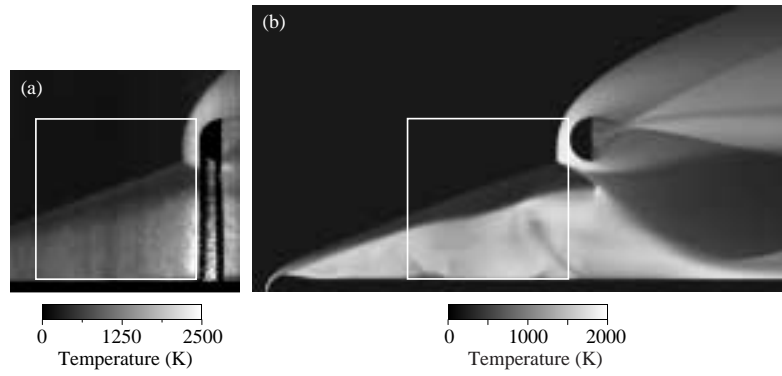


**Fig. 10.** Comparison between (a) experimental temperature measurement and (b) numerical simulation at the low enthalpy condition ( $d = 110$  mm); rectangles indicate common regions

## References

1. Hall JL (2000) A review of ballute technology for planetary aerocapture. IAA-L-1112, presented at the 4th IAA Conf Low Cost Planetary Missions, Laurel, Maryland, USA
2. Rasheed A, Fujii K, Valiferdowski B, Hornung HG (2000) Preliminary experimental investigation of the flow over a toroidal ballute. GALCIT Rep FM 00-4
3. Hornung HG (1992) Performance data of the new free-piston shock tunnel T5 at GALCIT. AIAA paper 92-3943
4. Houwing AFP, Isbister S, Lourel I, Eichmann TN, McIntyre TJ, Morgan RG (2001) Axi-symmetric shock-shock interaction and shock-induced separation in a hypersonic flow. In preparation
5. Sanderson SR (1995) Shock wave interaction in hypervelocity flow. Ph.D. dissertation, Caltech
6. Riabov VV (1999) Numerical study of hypersonic rarefied-gas flows about a torus. J Spacecraft Rockets 36(2):293-296
7. Fay J, Riddell FR (1958) Theory of stagnation point heat transfer in dissociated air. J Aeron Sci 25(2):73-85